Phase-dependent topological interface state and spatial adiabatic passage in a generalized Su-Schrieffer-Heeger model

Lei Du,[1] Jin-Hui Wu,[1,2,*] M. Artoni,[3,†] and G. C. La Rocca[4,‡]

[1]*Center for Quantum Sciences and School of Physics, Northeast Normal University, Changchun 130117, China*
[2]*State Key Laboratory of Quantum Optics and Quantum Optics Devices, Shanxi University, Taiyuan 030006, China*
[3]*Department of Engineering and Information Technology and Istituto Nazionale di Ottica (INO-CNR), Brescia University, 25133 Brescia, Italy*
[4]*Scuola Normale Superiore and CNISM, 56126 Pisa, Italy*

(Received 5 March 2019; published 12 July 2019)

We extend the Su-Schrieffer-Heeger model to include both an additional real intercell coupling and a complex intracell coupling whose phase can be interpreted as the Peierls phase associated with a synthetic gauge field. Using different Peierls phases, we can realize a heterostructure supporting a topologically protected interface state, depending on the existence of one trivial and two nontrivial phases of distinct winding numbers. The spatial adiabatic passage of this localized state from the inner interface to either open boundary can be attained simply by modulating the corresponding Peierls phase, while its decay or growth rate is controlled by the on-site parity-time symmetric loss and gain terms. Our results provide a scheme to achieve dynamical control of topologically protected states while being of potential interest to topological lasers with an adjustable spatial profile.

DOI: 10.1103/PhysRevA.100.012112

I. INTRODUCTION

As a new phase of matter, topological insulators (TI) are characterized by an insulating bulk and a conducting surface [1,2]. According to the conventional bulk-edge correspondence, one can observe gapless edge modes near the interface between a TI and a trivial medium. While in two-dimensional TIs waves typically propagate along the edges as chiral states, in one-dimensional TIs edge states are simply localized at the boundaries, decaying rapidly into the bulk. One crucial advantage of topologically protected edge states is that they are robust against fabrication imperfections and disorders. For Hermitian TIs, the bulk-edge correspondence is well explored and understood, and various topological invariants have been proposed to characterize distinct topological phases [3]. However, many realistic physical systems, such as open systems [4–7] and photonic systems with loss and/or gain [8–12], are described by non-Hermitian Hamiltonians, the topological properties of which are intensively being investigated [13]. Topological photonics, in particular, has attracted a great deal of interest accompanied with rapid progress [14,15]. The experimental realization of topological edge states in a lossy waveguide array [16] has revived the debate about the bulk-edge correspondence for non-Hermitian TIs, a notion that is reconsidered in systems exhibiting an anomalous localization or non-Hermitian skin effect, whereas in other instances it holds true as typically described by topological invariants [17–29]. Compared with condensed-matter electronic systems, photonic systems exhibit three major advantages in studying topological effects: first, in photonics, loss and gain are ubiquitous and can be controlled [30]; second, optical nonlinearities enable richer phenomena in topological photonics [31]; and third, due to various internal degrees of freedom, it is possible to realize synthetic dimensions in photonic systems [32]. To date, a lot of breakthroughs have been achieved based on such properties, such as optical delay lines with enhanced transport properties [33], backscattering-free edge states [34,35], and topological polaritons [36], to name a few. In particular, the concept of topological lasing has been put forth and demonstrated by exploiting the confinement of light to a topological protected edge mode in an active TI to achieve single-mode laser operation [37–42].

The tight-binding Su-Schrieffer-Heeger (SSH) model [43], which in its most basic version only includes a real intracell hopping term and a real nearest-neighbor intercell hopping term, has been widely studied as a one-dimensional prototype allowing for a nontrivial topological phase [44,45]. This model has been extended in a variety of Hermitian [46–49] and non-Hermitian forms [16,20,21,27,39–41,50–58]. In particular, the non-Hermitian extensions, which are also called complex SSH models, are a powerful platform for studying interactions of topological properties with non-Hermiticity, and many breakthroughs have been made based on them, such as anomalous edge states [21], non-Bloch bulk-edge correspondence [27], topological lasing [39–41], and spontaneous topological pumping [58]. Here, we consider a further extension of the non-Hermitian SSH model to include (i) a complex intracell hopping term, (ii) an additional intercell hopping term beyond the nearest-neighbor one, and (iii) non-Hermitian on-site loss and gain terms. The phase of the complex intracell hopping term (Peierls phase) can be tuned via a synthetic gauge field [32,59–66]. While loss and gain are needed for lasing action, the Peierls phase degree of freedom

*jhwu@nenu.edu.cn
†artoni@lens.unifi.it
‡larocca@sns.it

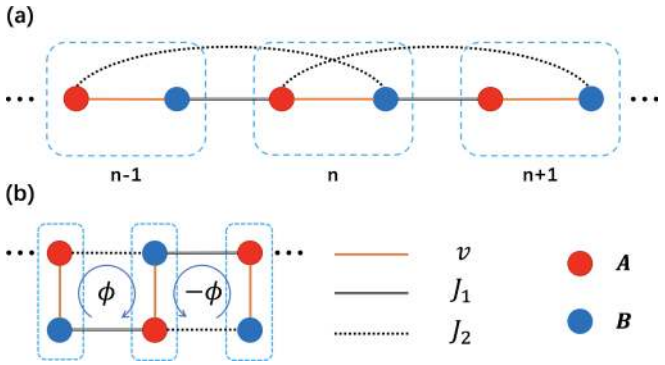

FIG. 1. (a) The schematic illustration of a generalized SSH model. (b) The equivalent ladder lattice of the SSH model in panel (a). While the intercell hopping terms J_1 and J_2 are real-valued, the intracell hopping term is complex with the modulus v (which will be taken as units of energies) and the Peierls phase ϕ. On-site loss and gain terms can be introduced in a balanced fashion on sites A and sites B, respectively, to realize a non-Hermitian $\mathcal{PT}$-symmetric system.

would be immaterial in the absence of the additional intercell coupling as discussed below. Thus, our extension represents the minimal SSH model apt to implement a topologically protected mode, the spatial profile of which can be controlled via the Peierls phase: by dividing a finite sample into two parts with different Peierls phases, we can observe a topologically protected mode at the interface which can be adiabatically transferred between the interface and one open boundary by adjusting the synthetic gauge field. During the process, this mode remains topologically protected because its eigenvalue does not merge into the bulk bands; moreover, in the presence of suitable loss and gain terms, we show that this adiabatic process also holds when the mode is amplified so that it is of potential interest in topological lasing with a tunable spatial profile, a highly sought-after feature for signal spatial encoding and broad-area emission [38,53].

The focus of the work is to elucidate the main features of the extended SSH model through a specific single-particle tight-binding Hamiltonian. Hence we are not committed in this paper to any particular platform for exploring the new topological physics associated with such an extension though possible settings are briefly suggested in Sec. IV. We also conclude with a summary in Sec. IV, after describing the details of our extended model in Sec. II and discussing the main results in Sec. III.

II. THE GENERALIZED SSH MODEL

We consider the generalized SSH model shown in Fig. 1(a) having two sites per unit cell, sites A (red) and B (blue), and three distinct hopping terms, the intracell coupling (orange solid line), the nearest-neighbor intercell coupling (J_1, gray solid line), and an additional next-nearest-neighbor intercell coupling (J_2, gray dotted line). While we assume both intercell hopping terms J_1 and J_2 to be real-valued, we consider a complex-valued intracell coupling of modulus v and a tunable Peierls phase ϕ, i.e., the intracell hopping term is $v_{AB} = v_{BA}^* = ve^{i\phi}$. In fact, this generalized SSH model is equivalent to a ladder lattice with sites A and B arranged alternately around each plaquette as shown in Fig. 1(b), and a tunable synthetic gauge field enables the control of the phase ϕ. Here, the synthetic gauge field should be opposite in adjacent plaquettes in order to introduce uniform Peierls phase in Fig. 1(a). Unlike other SSH models [27,53,55], we note that all hopping terms preserve Hermiticity. Since a nonvanishing average value of gain (or loss) would not affect the spatial profile of the edge mode we are interested in [40], we choose to introduce loss on every A site and gain on every B site in a balanced fashion. In this way, our model respects either chiral or parity-time ($\mathcal{PT}$) symmetry when the loss and gain rate is taken to be, respectively, vanishing or nonvanishing.

Since the homogeneous model is translationally invariant, using the Bloch theorem, the k-space Hamiltonian is obtained as

$$H(k) = h_x(k)\sigma_x + h_y(k)\sigma_y + h_z\sigma_z, \tag{1}$$

with

$$h_x(k) = v\cos\phi + (J_1 + J_2)\cos k,$$
$$h_y(k) = -v\sin\phi + (J_1 - J_2)\sin k,$$
$$h_z = -i\gamma.$$

Here, σ_j ($j = x$, y, and z) are the Pauli matrices and k is the dimensionless scaled Bloch wave number in the first Brillouin zone ($-\pi \leqslant k < \pi$). While h_x and h_y are real and k-dependent, h_z is purely imaginary and constant, with a positive value of γ corresponding to loss on the A sites and gain on the B sites. Then, the symmetries mentioned above lead to the pseudo-anti-Hermiticity of $H(k)$ with $\sigma_z H(k)^\dagger \sigma_z = -H(k)$ [18,52], as well as to the so-called chiral-time symmetry [40] of $H(k)$, which can be represented by the antiunitary operator $\sigma_x\mathcal{K}$, $\mathcal{K}$ being the complex conjugation, with $[\sigma_x\mathcal{K}, H(k)] = 0$. The eigenvalues of $H(k)$ are given by

$$E_\pm(k) = \pm\sqrt{-\gamma^2 + v^2 + J_1^2 + J_2^2 + 2vJ_1\cos(k+\phi) + 2vJ_2\cos(k-\phi) + 2J_1J_2\cos(2k)}, \tag{2}$$

which satisfy $E_+(k) = -E_-(k)$ and are either real or purely imaginary. Equation (2) also shows that the energy bands have a nontrivial dependence on the Peierls phase ϕ only when both J_1 and J_2 are present: if J_2 vanishes, the only effect of ϕ is a rigid displacement of the bands in the k space. As a matter of fact, in the absence of J_2, the phase ϕ could always be gauged away via a redefinition of the basis states [45], as also evident from the fact that in this case there are no closed plaquettes in Fig. 1(b).

Differently from some non-Hermitian models [21,23,27,53] while similarly to others [16,40,50,52,57], the present generalized SSH model does not exhibit the non-Hermitian skin effect. Thus, the characterization of its nontrivial topological properties, in terms of the winding

number corresponding to the non-Hermitian extension [19,67] of the Zak phase [44,68], can provide guidance for the realization of heterostructures with spatially tunable and robust localized modes suitable for topological lasing [40]. We indicate with $\langle\varphi_\alpha(k)|$ and $|\psi_\alpha(k)\rangle$ the left and right eigenvectors of $H(k)$ corresponding to the eigenvalue $E_\alpha(k)$, where $\alpha = \pm$ labels the energy bands as in Eq. (2), with the biorthogonal normalization $\langle\varphi_\alpha(k)|\psi_\beta(k)\rangle = \delta_{\alpha,\beta}$ [69]. Then, the complex single-band Zak phase (in units of π) is given by

$$w_\alpha = \frac{1}{\pi}\int_{-\pi}^{\pi} dk\ \langle\varphi_\alpha|i\,\partial_k|\psi_\alpha\rangle. \tag{3}$$

For a model of the form of Eq. (1), the above formula can be analytically rewritten as [55]

$$w_\alpha = \frac{1}{2\pi}\int_{-\pi}^{\pi} dk \frac{h_x\partial_k h_y - h_y\partial_k h_x}{E_\alpha(k)[E_\alpha(k) - h_z]}, \tag{4}$$

and the global Zak phase $w_{\rm tot} = w_+ + w_-$, a proper topological invariant for our non-Hermitian system [16,19,52,57], making use of Eq. (2) becomes simply

$$w_{\rm tot} = \frac{1}{\pi}\int_{-\pi}^{\pi} dk \frac{h_x\partial_k h_y - h_y\partial_k h_x}{h_x^2 + h_y^2}. \tag{5}$$

It is noticeable that the value of $w_{\rm tot}$ equals twice the single-band Zak phase of the parent Hermitian model [i.e., the one obtained by setting $h_z = 0$ in Eq. (1)] which is the same for both bands and takes integer values. Thus, the topologically distinct phases of the present generalized SSH model are inherited from its parent Hermitian one, similarly to other instances of non-Hermitian systems [19,50,57]. In particular, the value of γ, which characterizes the amount of loss and gain introduced in the Hamiltonian and determines its $\mathcal{PT}$-symmetry transition [70], does not affect the topological phase transitions. In the following, our strategy is (A) to harness the degree of freedom provided by the Peierls phase ϕ in order to realize a heterostructure between topologically distinct phases; (B) to assess how the heterostructure is affected by loss and gain allowing for topological lasing; (C) to implement the control of the spatial profile of the topologically protected mode; and, finally, (D) to show that the energy of this mode and its spatial adiabatic passage are robust against disorder.

III. RESULTS AND DISCUSSION

A. Topological heterostructure

We start by assessing how the Peierls phase ϕ affects the topological properties of the generalized SSH model which, as discussed above, do not depend on the loss and gain terms proportional to γ. We plot in Fig. 2 the winding number $w \equiv w_{\rm tot}/2$ for different parameter values. As shown in Fig. 2(a), one can observe in a wide range of parameters three topological phases, characterized by $w = \pm 1$ and $w = 0$, respectively. While $w = 0$ corresponds to a topologically trivial phase with no edge states, $w = \pm 1$ correspond to two distinct topologically nontrivial phases with different types of edge states. In fact, similar results have already been discussed in Refs. [47,48]. Here, we show in Figs. 2(b) and 2(c) that the topological phase diagram can be changed by adjusting ϕ,

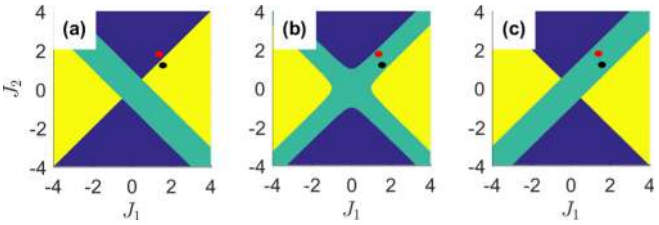

FIG. 2. Topological phase diagrams of the generalized SSH model with (a) $\phi = 0$, (b) $\phi = \pi/4$, and (c) $\phi = \pi/2$. In each panel, the yellow, blue, and green regions correspond to the winding numbers $w = 1$, $w = -1$, and $w = 0$, respectively. The red/gray (black) dots in panels (a)–(c) correspond to $J_1 = 1.4$ and $J_2 = 1.8$ ($J_1 = 1.5$ and $J_2 = 1.2$), with $v = 1$ being taken as the unit of energies.

being the parameter range of the topological trivial phase with $w = 0$ most sensitive to ϕ. We conclude that in the present extension of the SSH model ($J_2 \neq 0$) the topological phase can be controlled by adjusting the value of ϕ.

Next, we consider a heterostructure between two aforementioned generalized SSH models having different values of ϕ, which can be obtained by dividing the whole sample into two halves subject to distinct synthetic gauge fields. To be definite, here we consider a finite generalized SSH model with 150 unit cells (300 sites), assuming that the left part contains the first 75 unit cells with the Peierls phase ϕ_1, while the right part contains the last 75 unit cells with the Peierls phase ϕ_2. If $\phi_1 = \phi_2$, the model recovers a (finite) homogeneous structure.

According to the specific results in Fig. 2, if $\phi_1 \neq \phi_2$, the left and right parts of the model may be topologically distinct, and thereby we expect a topologically protected state localized at the interface. In particular, choosing the parameters corresponding to the black dots in Figs. 2(a) and 2(b) and letting $\phi_1 = 0$ and $\phi_2 = \pi/2$, the left part is topologically nontrivial with $w = 1$ while the right part is topologically trivial with $w = 0$.

Considering first the Hermitian case with $\gamma = 0$, the presence of a zero mode localized at the interface is shown in Fig. 3. In Fig. 3(a), we plot the energy spectrum of a finite heterostructure with open boundary conditions at the outer edges and find that there are two zero modes residing within the band gap [see the two orange (gray) dots], as typical of topological edge states. Indeed, as shown in Fig. 3(b), the two degenerate modes correspond to a localized state at the left edge and a localized state at the middle interface. In Figs. 3(c) and 3(d), we further demonstrate the zoomed-in images of the edge and interface states, respectively. They show that the left edge state resides only on A sites (odd number of sites), while the interface state resides only on B sites (even number of sites). This is much similar to the case of a standard SSH model, in which the two edge states reside on different sublattices, respectively. In contrast, if we choose the coupling parameters corresponding to the red (gray) dots in Fig. 2, the winding number of the left part becomes $w = -1$, while that of the right part remains $w = 0$. In this case, the left edge (interface) state resides only on B (A) sites (not shown here).

B. Topological modes with gain and loss

We further extend the above results to the non-Hermitian regime by introducing balanced loss and gain terms

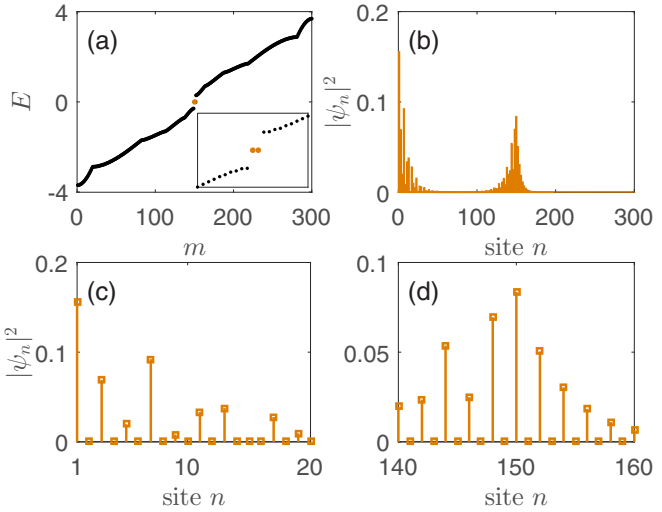

FIG. 3. (a) The energy spectrum of a finite heterostructure based on the Hermitian ($\gamma = 0$) generalized SSH model with $v = 1$, $J_1 = 1.5$, $J_2 = 1.2$, $\phi_1 = 0$, and $\phi_2 = \pi/2$; the inset shows in detail the two orange (gray) dots correspond to the degenerate left edge and interface states; m labels the eigenvalues in order of increasing energy. (b) The spatial profiles of the edge and interface states in this case. (c) and (d) The zoomed-in images of the edge and interface states, respectively.

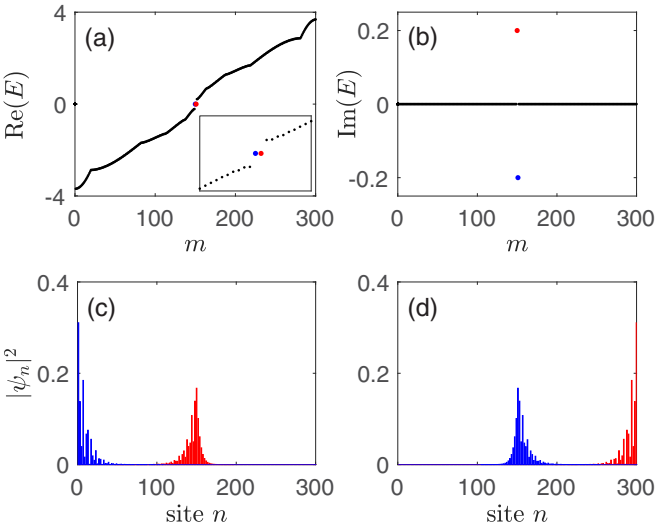

FIG. 4. The real (a) and imaginary (b) parts of the energy spectrum of the $\mathcal{PT}$-symmetric heterostructure, respectively, with $\phi_1 = 0$ and $\phi_2 = \pi/2$. The spatial profiles of the edge and interface states are depicted in panel (c) with $\phi_1 = 0$ and $\phi_2 = \pi/2$ and in panel (d) with $\phi_1 = \pi/2$ and $\phi_2 = 0$. Here, the profiles depicted by red (gray) lines correspond to growing states, while those depicted by blue (dark gray) lines correspond to damped states. In particular, the edge (blue) and interface (red) states in panel (c) correspond to the blue and red dots in panels (a) and (b), respectively. Other parameters are the same as those in Fig. 3 except $\gamma = 0.2$.

alternately on the A and B sites. According to Eqs. (3)–(5) and related discussions, such an introduction does not alter the topological phase transitions, so it is still viable to find an interface state with its spatial profile controlled by the Peierls phase. We start showing the complex energy spectrum of the heterostructure in Figs. 4(a) and 4(b). Clearly, there are two midgap modes, the eigenvalues of which have zero-valued real parts and opposite imaginary parts ($\pm\gamma$). As shown in Fig. 4(c), the two modes correspond, respectively, to a damped left edge state with a negative imaginary eigenvalue and a growing interface state with a positive imaginary eigenvalue. Recently, it has been proved that an edge mode whose eigenvalue has a positive imaginary part can be used for realizing single-mode topological lasing [37–42,57] that is robust against local perturbations. Generally, an edge (interface) state can be set to be either damped or growing by a suitable choice of the loss and gain terms [20,24]. However, we anticipate here that this can also be accomplished via a dynamic modulation of the Peierls phases. For instance, if we exchange the values of ϕ_1 and ϕ_2 in Fig. 4(c) to make the left (right) half topologically trivial (nontrivial) instead, the interface state becomes damped and a growing edge state arises at the right open boundary, as shown in Fig. 4(d). In the latter case, the interface state resides only on the A sites with loss, while the right edge state resides only on the B sites with gain.

To investigate the $\mathcal{PT}$-symmetry transitions of the non-Hermitian heterostructure, we plot in Fig. 5 its energy spectrum as a function of γ. The vertical lines in Fig. 5 correspond to the case shown in Fig. 4, the different shading along this line in Fig. 5(a) representing the varying density of states of the spectrum in Fig. 4(a). Since the introduction of γ does not affect the topological phases, no matter how large γ is, there are always only two topologically protected modes (one edge and one interface) with imaginary eigenvalues $\pm i\gamma$. It is also clear that, as γ increases, the real part of the spectrum as well as the band gap will shrink, while the imaginary part will widen gradually. We find in particular two critical values, $\gamma_{c1} = 0.30$ and $\gamma_{c2} = 3.65$, characterizing the $\mathcal{PT}$-symmetry transitions in this figure. For $\gamma < \gamma_{c1}$, the

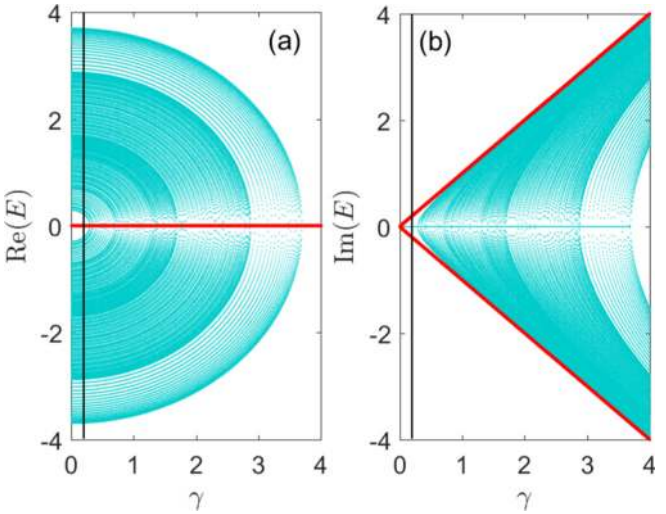

FIG. 5. The real (a) and imaginary (b) parts of the energy spectrum of the $\mathcal{PT}$-symmetric heterostructure as functions of γ with $\phi_1 = 0$ and $\phi_2 = \pi/2$. The red (gray) lines depict the eigenvalues of the edge and interface states. Other parameters are the same as those in Fig. 4.

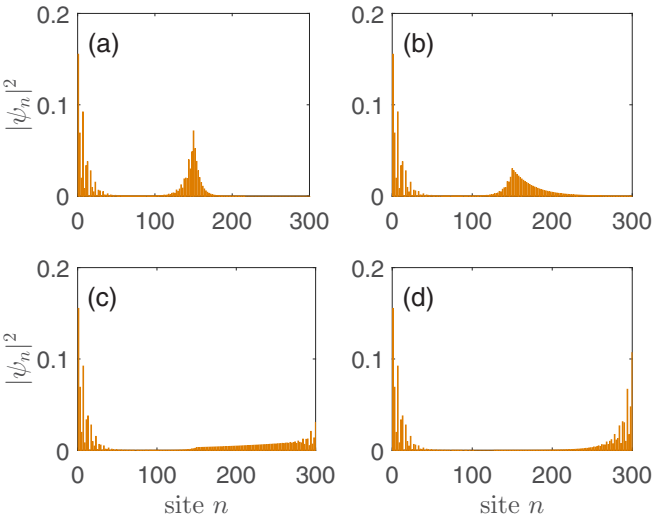

FIG. 6. The spatial profiles of the edge and interface states for the finite heterostructure based on the Hermitian ($\gamma = 0$) generalized SSH model with (a) $\phi_2 = \pi/4$, (b) $\phi_2 = \pi/8$, (c) $\phi_2 = \pi/12$, and (d) $\phi_2 = \pi/20$. Other parameters are the same as those in Fig. 3.

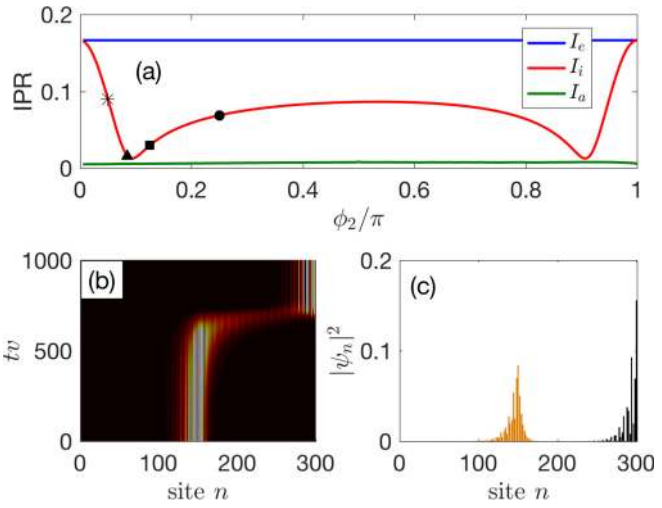

FIG. 7. (a) The IPRs of the edge and interface states, and the averaged IPR of all bulk states of a finite heterostructure based on the Hermitian ($\gamma = 0$) generalized SSH. The dot, the square, the triangle, and the asterisk correspond to $\phi_2 = \pi/4$, $\pi/8$, $\pi/12$, and $\pi/20$, respectively. (b) A dynamic SAP of the interface state shown in Fig. 3(b). (c) The intensity profiles of the initial (orange/gray) and the final (black) states in panel (b). Other parameters are the same as those in Fig. 3.

eigenvalues of all bulk states are real, while those of the edge and interface states are imaginary and conjugate. For $\gamma_{c1} < \gamma < \gamma_{c2}$, part of the bulk states become $\mathcal{PT}$-symmetry-broken (i.e., their eigenvalues become imaginary) and the number of these bulk states increases with γ. This is consistent with previous works [71,72], where relevant systems undergo $\mathcal{PT}$-symmetry breaking immediately once a nonvanishing γ is introduced because the eigenvalues of the edge modes acquire imaginary parts. Further increasing γ, we can see a second phase transition at $\gamma = \gamma_{c2}$, above which all eigenvalues become imaginary. It is worth noting that the $\mathcal{PT}$-symmetry breaking will induce a change from single edge-mode lasing to multimode lasing [40].

C. Spatial adiabatic passage

In this section we show that the spatial profile of the interface state can be controlled via the Peierls phase. As shown in Figs. 6(a)–6(c), if we reduce ϕ_2 from $\pi/2$ gradually, the interface state becomes more and more extended at first. With small enough ϕ_2, its wave function extends into the bulk of the right part, as shown in Fig. 6(c). If ϕ_2 further decreases, we find from Fig. 6(d) that the interface state eventually becomes localized to the right open boundary. In particular, when ϕ_2 vanishes, the heterostructure reduces to a homogeneous sample with the winding number $w = 1$, and thereby one can observe two chiral edge states localized at the left and right boundaries, respectively. Notice that as ϕ_2 changes, the interface state remains on the same sublattice (i.e., it always resides on B sites here), even when it becomes extended during the process. At the same time, the left edge state is insensitive to ϕ_2.

We gain further insight by introducing the inverse participation ratio (IPR) [73,74] of an eigenstate $\psi = \sum_n \psi_n$,

$$I = \frac{\sum_n |\psi_n|^4}{\left(\sum_n |\psi_n|^2\right)^2}, \tag{6}$$

which is a measure of the state's localization whereby larger IPRs correspond to stronger localization. In one-dimensional systems, the IPR of an extended state roughly equals the inverse of the system length. In Fig. 7(a), we plot the IPRs of the edge and interface states denoted by I_e and I_i, respectively, as well as the average of the IPRs of all bulk states, denoted by I_a. The variation of I_i indicates that the interface state becomes at first more and more extended as ϕ_2 decreases from $\pi/2$ until I_i reaches its minimum at around $\phi_2 = \pi/10$. With ϕ_2 further decreasing, the interface state rapidly becomes localized again. In particular, if $\phi_2 = 0$, the heterostructure reduces to a homogeneous sample and thereby the interface state becomes the standard right edge state, possessing the identical IPR with the left edge state. The dot, the square, the triangle, and the asterisk correspond to I_i values of the interface states in Figs. 6(a)–6(d), respectively. We also find that the left edge state is completely insensitive to ϕ_2 with a large I_e, while the bulk states are almost insensitive to ϕ_2 with a roughly vanishing I_a.

According to the adiabatic theorem [75,76], a system will remain in its instantaneous eigenstate for (i) slow enough perturbations and for (ii) a large enough gap between the corresponding eigenvalue and the rest of the spectrum. Thus we foresee as viable the spatial adiabatic passage (SAP) of a topologically protected mode [77,78] through slow changes of the Peierls phase ϕ. In this case excitations can be coherently transferred between spatially separated localized states with high efficiency and strong robustness. SAP was initially proposed following the idea of stimulated Raman adiabatic passage in three-level atomic systems and has been extended to optical systems with more than three coupled waveguides [79–81]. In our model, SAP is achieved by initially exciting a zero-energy mode and then by adiabatically changing the

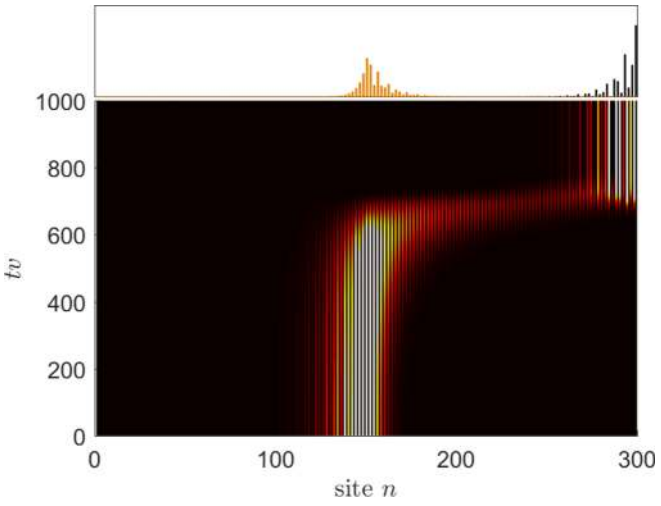

FIG. 8. A dynamic SAP of the growing interface state in Fig. 4(c) with spatial profiles of the initial (orange/gray) and final (black) states shown in the top inset. The final state is amplified similarly to the edge state in Fig. 4(d). Other parameters are the same as those in Fig. 4.

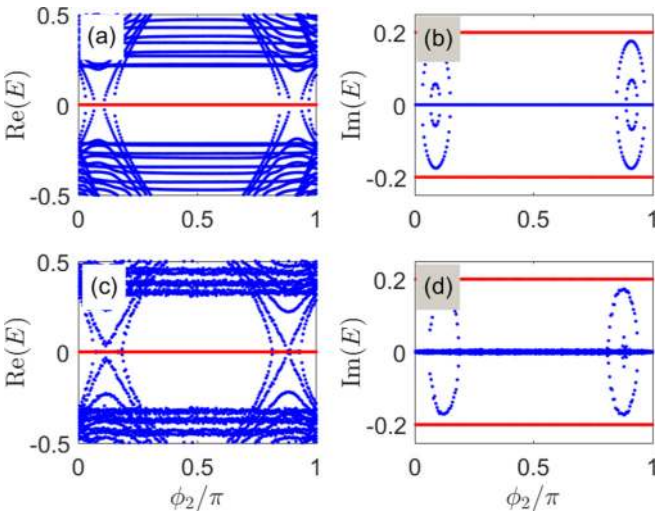

FIG. 9. The real (a) and imaginary (b) parts of the energy spectrum of the $\mathcal{PT}$-symmetric heterostructure as functions of ϕ_2 without disorder. The real (c) and imaginary (d) parts of the energy spectrum of the $\mathcal{PT}$-symmetric heterostructure as functions of ϕ_2 with disorder described by $\{\delta v_n,\ \delta J_{1,n},\ \delta J_{2,n}\} \in [-0.2,\ 0.2]$. The red lines depict the eigenvalues of the edge and interface states. Other parameters are the same as in those Fig. 3, except for $\gamma = 0.2$.

Peierls phase of the half part of the sample through which it is to be transferred. Here we demonstrate this dynamic process in Fig. 7(b) by using the interface state shown in Fig. 3(b) as the initial state and assuming $\phi_2(t) = \pi/2 - \pi t v/1600$ for $tv < 800$ and $\phi_2(t) \equiv 0$ for $tv \geqslant 800$. It is clear that the interface state is adiabatically transferred to the right open boundary and thereby evolves into the right edge state. In Fig. 7(c), we plot the spatial profiles of the initial interface and the final right edge states. These results are consistent with those in Fig. 4 and confirm that the SAP is highly efficient.

Moreover, an effective SAP can also be realized for the non-Hermitian case. We demonstrate in Fig. 8 how the growing interface state shown in Fig. 4(c) can be adiabatically transferred to the right open boundary in the same way as in Fig. 7(b). Note that the intensity profiles here have been normalized by $\sum_n |\psi_n(t)|^2$. The spatial profiles of the initial and final states in the top inset indicate that the SAP in this case maintains high efficiency. In non-Hermitian systems, there are in general limitations to the observation of adiabatic transport as, e.g., when state switching and piecewise adiabatic following occur [82–86]. Adiabatic passage of damped states is in our case unfeasible owing to the fact that, while these states vanish with time, nonadiabatic processes may populate other states undergoing amplification, as seen for instance in Ref. [58]. Conversely, the adiabatic transport shown in Fig. 8 occurs as favored by the fact that, for positive γ's ($\gamma < \gamma_{c1}$), the state undergoing SAP remains efficiently amplified through the end of the process. Other states possibly seeded by nonadiabatic processes are instead damped. As we are not concerned here with the actual determination of the threshold for a potential lasing action based on such a state, we do not consider gain saturation or nonlinear effects which would eventually affect the propagation of the amplified mode. The relevant message conveyed by the above results is that the spatial profile of the mode potentially suitable for topological lasing can be dynamically controlled via the Peierls phase.

D. Robustness against disorder

Finally, we aim to show that both the edge and the interface states remain topologically protected during a SAP so that they are robust against certain types of disorder. In Figs. 9(a) and 9(b), we plot the complex energy spectrum as a function of ϕ_2 with its real part only shown around the energy gap. Figure 9(b) shows that the eigenvalues of some bulk states become imaginary in the vicinities of $\phi_2 = 0.1\pi$ and 0.9π, while all of them are real elsewhere. So changing ϕ_2 may lead to $\mathcal{PT}$-symmetry transitions while the $\mathcal{PT}$-broken regions may shrink or even disappear if we reduce γ. Most importantly, though the interface state becomes extended in its wave function during a SAP, its eigenvalue remains invariant (see the red lines) so that the SAP in our model is topologically protected. This is quite different from other instances of adiabatic pumping [87], whereby during the process the edge state acquires a bulklike character in terms of both its wave function and eigenvalue, the latter shifting and tending to merge into the bulk spectrum. One of the most intriguing characteristics of the topologically protected states is that they are robust against imperfections. To prove this, we introduce disorders in the couplings, i.e., $v \to 1 + \delta v_n$ and $J_\beta \to J_\beta + \delta J_{\beta n}$ ($\beta = 1$ and 2), with $-0.2 \leqslant \delta v_n,\ \delta J_{1n}$, and $\delta J_{2n} \leqslant 0.2$ being three independent stochastic (real) variables. In Figs. 9(c) and 9(d), we can find that the edge and interface states are immune to disorder, i.e., their eigenvalues are essentially identical to those in Figs. 9(a) and 9(b). Moreover, we have numerically verified that the edge and interface states also resist real-valued on-site disorders, i.e., $\gamma \to \gamma + i\Delta_n$, with $-0.2 \leqslant \Delta_n \leqslant 0.2$. If we introduce complex-valued on-site disorders instead, the real parts of their eigenvalues do not change, while the imaginary parts undergo limited random shifts (not shown here).

IV. CONCLUSIONS

The one-dimensional Su-Schrieffer-Heeger model, one among the simplest to host topological properties, has long served as an archetype of a topological structure [45]. Our generalized SSH model, with two distinct real intercell couplings yet a *complex* intracell coupling, is found to exhibit a trivial and two nontrivial topological phases characterized by the non-Hermitian winding numbers $w = \{0, \pm 1\}$, respectively. Although these are not affected by the degree of non-Hermiticity, yet they are sensitive to the phase of the hopping term (Peierls phase). A topologically protected mode, lying at the interface between the two halves of a structure bearing different Peierls phases, is seen to be robust against disorder and of potential interest to topological lasing. Dynamic control of the spatial profile of this zero mode can be efficiently achieved through spatial adiabatic passage.

The emergence of topological phenomena in a simple one-dimensional setting has clearly inspired a number of experimental investigations using various platforms such as superconducting qubits [64], ultracold atoms [88,89], and resistor-inductor-capacitor circuits [90]. One-dimensional periodic [51] and quasiperiodic [87] waveguide arrays have recently provided a complementary window into the physics of topological photonic structures. Within such a framework, aspects of our model can be achieved with promising platforms based on coupled ring resonators subject to synthetic gauge fields. Such fields can be realized and even tuned via thermal or electro-optic modulators [33,65,66] or more versatile couplers [62,63], some of which would allow for all-optical control as well as time-dependent *in situ* tunability [63]. It is also worthwhile stressing that all our results hinge on the tight-binding Hamiltonian of Eq. (1) with a variable phase ϕ as a control parameter. Hence our results could be implemented in non-Hermitian tight-binding network systems [91] without resorting to the notion of synthetic gauge fields.

ACKNOWLEDGMENTS

This work is supported by the National Natural Science Foundation of China (Grants No. 10534002 and No. 11674049), the Cooperative Program by the Italian Ministry of Foreign Affairs and International Cooperation (Grant No. PGR00960) and the National Natural Science Foundation of China (Grant No. 11861131001), and the Program of State Key Laboratory of Quantum Optics and Quantum Optics Devices (Grant No. KF201807). We also thank S. Chesi, Y. D. Wang, and Y. Zhang for helpful discussions.

[1] M. Z. Hasan and C. L. Kane, Colloquium: Topological insulators, Rev. Mod. Phys. **82**, 3045 (2010).

[2] X.-L. Qi and S.-C. Zhang, Topological insulators and superconductors, Rev. Mod. Phys. **83**, 1057 (2011).

[3] B. A. Bernevig and T. L. Hughes, *Topological Insulators and Topological Superconductors* (Princeton University, Princeton, NJ, 2013).

[4] Y. Choi, S. Kang, S. Lim, W. Kim, J.-R. Kim, J.-H. Lee, and K. An, Quasieigenstate Coalescence in an Atom-Cavity Quantum Composite, Phys. Rev. Lett. **104**, 153601 (2010).

[5] S. Diehl, E. Rico, M. A. Baranov, and P. Zoller, Topology by dissipation in atomic quantum wires, Nat. Phys. **7**, 971 (2011).

[6] T. E. Lee and C.-K. Chan, Heralded Magnetism in Non-Hermitian Atomic Systems, Phys. Rev. X **4**, 041001 (2014).

[7] H. Cao and J. Wiersig, Dielectric microcavities: Model systems for wave chaos and non-Hermitian physics, Rev. Mod. Phys. **87**, 61 (2015).

[8] K. G. Makris, R. El-Ganainy, D. N. Christodoulides, and Z. H. Musslimani, Beam Dynamics in $\mathcal{PT}$ Symmetric Optical Lattices, Phys. Rev. Lett. **100**, 103904 (2008).

[9] S. Longhi, Bloch Oscillations in Complex Crystals with $\mathcal{PT}$ Symmetry, Phys. Rev. Lett. **103**, 123601 (2009).

[10] H. Hodaei, M.-A. Miri, M. Heinrich, D. N. Christodoulides, and M. Khajavikhan, Parity-time-symmetric microring lasers, Science **346**, 975 (2014).

[11] C. Poli, M. Bellec, U. Kuhl, F. Mortessagne, and H. Schomerus, Selective enhancement of topologically induced interface states in a dielectric resonator chain, Nat. Commun. **6**, 6710 (2015).

[12] K. Takata and M. Notomi, Photonic Topological Insulating Phase Induced Solely by Gain and Loss, Phys. Rev. Lett. **121**, 213902 (2018).

[13] V. M. M. Alvarez, J. E. B. Vargas, M. Berdakin, and L. E. F. Foa Torres, Topological states of non-Hermitian systems, Eur. Phys. J. Spec. Top. **227**, 1295 (2018).

[14] A. B. Khanikaev, S. H. Mousavi, W.-K. Tse, M. Kargarian, A. H. MacDonald, and G. Shvets, Photonic topological insulators, Nat. Mater. **12**, 233 (2013).

[15] T. Ozawa, H. M. Price, A. Amo, N. Goldman, M. Hafezi, L. Lu, M. C. Rechtsman, D. Schuster, J. Simon, O. Zilberberg, and I. Carusotto, Topological photonics, Rev. Mod. Phys. **91**, 015006 (2019).

[16] S. Weimann, M. Kremer, Y. Plotnik, Y. Lumer, S. Nolte, K. G. Makris, M. Segev, M. C. Rechtsman, and A. Szameit, Topologically protected bound states in photonic parity-time-symmetric crystals, Nat. Mater. **16**, 433 (2017).

[17] Y. C. Hu and T. L. Hughes, Absence of topological insulator phases in non-Hermitian PT-symmetric Hamiltonians, Phys. Rev. B **84**, 153101 (2011).

[18] K. Esaki, M. Sato, K. Hasebe, and M. Kohmoto, Edge states and topological phases in non-Hermitian systems, Phys. Rev. B **84**, 205128 (2011).

[19] S.-D. Liang and G.-Y. Huang, Topological invariance and global Berry phase in non-Hermitian systems, Phys. Rev. A **87**, 012118 (2013).

[20] H. Schomerus, Topologically protected midgap states in complex photonic lattices, Opt. Lett. **38**, 1912 (2013).

[21] T. Lee, Anomalous Edge State in a Non-Hermitian Lattice, Phys. Rev. Lett. **116**, 133903 (2016).

[22] D. Leykam, K. Y. Bliokh, C. Huang, Y. D. Chong, and F. Nori, Edge Modes, Degeneracies, and Topological Numbers in Non-Hermitian Systems, Phys. Rev. Lett. **118**, 040401 (2017).

[23] Y. Xiong, Why does bulk boundary correspondence fail in some non-Hermitian topological models, J. Phys. Commun. **2**, 035043 (2018).

[24] C. Yuce, Edge states at the interface of non-Hermitian systems, Phys. Rev. A **97**, 042118 (2018).

[25] F. K. Kunst, E. Edvardsson, J. C. Budich, and E. J. Bergholtz, Biorthogonal Bulk-Boundary Correspondence in Non-Hermitian Systems, Phys. Rev. Lett. **121**, 026808 (2018).

[26] Z. Gong, Y. Ashida, K. Kawabata, K. Takasan, S. Higashikawa, and M. Ueda, Topological Phases of Non-Hermitian Systems, Phys. Rev. X **8**, 031079 (2018).

[27] S. Yao and Z. Wang, Edge States and Topological Invariants of Non-Hermitian Systems, Phys. Rev. Lett. **121**, 086803 (2018).

[28] L. Jin and Z. Song, Bulk-boundary correspondence in a non-Hermitian system in one dimension with chiral inversion symmetry, Phys. Rev. B **99**, 081103(R) (2019).

[29] M. Silveirinha, Topological theory of non-Hermitian photonic systems, Phys. Rev. B **99**, 125155 (2019).

[30] L. Feng, R. El-Ganainy, and L. Ge, Non-Hermitian photonics based on parity-time symmetry, Nat. Photonics **11**, 752 (2017).

[31] Y. Lumer, Y. Plotnik, M. C. Rechtsman, and M. Segev, Self-Localized States in Photonic Topological Insulators, Phys. Rev. Lett. **111**, 243905 (2013).

[32] L. Yuan, Q. Lin, M. Xiao, and S. Fan, Synthetic dimension in photonics, Optica **5**, 1396 (2018).

[33] M. Hafezi, E. A. Demler, M. D. Lukin, and J. M. Taylor, Robust optical delay lines with topological protection, Nat. Phys. **7**, 907 (2011).

[34] Z. Wang, Y. Chong, J. D. Joannopoulos, and M. Soljačić, Observation of unidirectional backscattering-immune topological electromagnetic states, Nature (London) **461**, 772 (2009).

[35] M. Hafezi, S. Mittal, J. Fan, A. Migdall, and J. M. Taylor, Imaging topological edge states in silicon photonics, Nat. Photonics **7**, 1001 (2013).

[36] T. Karzig, C.-E. Bardyn, N. H. Lindner, and G. Refael, Topological Polaritons, Phys. Rev. X **5**, 031001 (2015).

[37] L. Pilozzi and C. Conti, Topological lasing in resonant photonic structures, Phys. Rev. B **93**, 195317 (2016).

[38] L. Ge, Symmetry-protected zero-mode laser with a tunable spatial profile, Phys. Rev. A **95**, 023812 (2017).

[39] P. St-Jean, V. Goblot, E. Galopin, A. Lemaitre, T. Ozawa, L. Le Gratiet, I. Sagnes, J. Bloch, A. Amo, Lasing in topological edge states of a one-dimensional lattice, Nat. Photonics **11**, 651 (2017).

[40] M. Parto, S. Wittek, H. Hodaei, G. Harari, M. A. Bandres, J. Ren, M. C. Rechtsman, M. Segev, D. N. Christodoulides, and M. Khajavikhan, Edge-Mode Lasing in 1D Topological Active Arrays, Phys. Rev. Lett. **120**, 113901 (2018).

[41] H. Zhao, P. Miao, M. H. Teimourpour, S. Malzard, R. El-Ganainy, H. Schomerus, and L. Feng, Topological hybrid silicon microlasers, Nat. Commun. **9**, 981 (2018).

[42] G. Harari, M. A. Bandres, Y. Lumer, M. C. Rechtsman, Y. D. Chong, M. Khajavikhan, D. N. Christodoulides, and M. Segev, Topological insulator laser: Theory, Science **359**, eaar4003 (2018).

[43] W. P. Su, J. R. Schrieffer, and A. J. Heeger, Solitons in Polyacetylene, Phys. Rev. Lett. **42**, 1698 (1979).

[44] P. Delplace, D. Ullmo, and G. Montambaux, Zak phase and the existence of edge states in graphene, Phys. Rev. B **84**, 195452 (2011).

[45] J. K. Asboth, L. Oroszlany, and A. Palyi, *A Short Course on Topological Insulators*, Lecture Notes in Physics, Vol. 919 (Springer International, Cham, 2016).

[46] L.-H. Li, Z.-H. Xu, and S. Chen, Topological phases of generalized Su-Schrieffer-Heeger models, Phys. Rev. B **89**, 085111 (2014).

[47] C. Li, S. Lin, G. Zhang, and Z. Song, Topological nodal points in two coupled Su-Schrieffer-Heeger chains, Phys. Rev. B **96**, 125418 (2017).

[48] X.-W. Xu, Y.-J. Zhao, H. Wang, A.-X. Chen, and Y.-X. Liu, Generalized Su-Schrieffer-Heeger model in one dimensional optomechanical arrays, arXiv:1807.07880.

[49] F. Mei, G. Chen, L. Tian, S.-L. Zhu, and S. Jia, Robust quantum state transfer via topological edge states in superconducting qubit chains, Phys. Rev. A **98**, 012331 (2018).

[50] M. S. Rudner and L. S. Levitov, Topological Transition in a Non-Hermitian Quantum Walk, Phys. Rev. Lett. **102**, 065703 (2009).

[51] J. M. Zeuner, M. C. Rechtsman, Y. Plotnik, Y. Lumer, S. Nolte, M. S. Rudner, M. Segev, and A. Szameit, Observation of a Topological Transition in the Bulk of a Non-Hermitian System, Phys. Rev. Lett. **115**, 040402 (2015).

[52] S. Lieu, Topological phases in the non-Hermitian Su-Schrieffer-Heeger model, Phys. Rev. B **97**, 045106 (2018).

[53] S. Longhi, Non-Hermitian gauged topological laser arrays, Ann. Phys. (Berlin) **530**, 1800023 (2018).

[54] F. Dangel, M. Wagner, H. Cartarius, J. Main, and G. Wunner, Topological invariants in dissipative extensions of the Su-Schrieffer-Heeger model, Phys. Rev. A **98**, 013628 (2018).

[55] H. Jiang, C. Yang, and S. Chen, Topological invariants and phase diagrams for one-dimensional two-band non-Hermitian systems without chiral symmetry, Phys. Rev. A **98**, 052116 (2018).

[56] L.-J. Lang, Y. Wang, H. Wang, and Y. D. Chong, Effects of non-Hermiticity on Su-Schrieffer-Heeger defect states, Phys. Rev. B **98**, 094307 (2018).

[57] M. Pan, H. Zhao, P. Miao, S. Longhi, and L. Feng, Photonic zero mode in a non-Hermitian photonic lattice, Nat. Commun. **9**, 1308 (2018).

[58] C. Yuce, Spontaneous topological pumping in non-Hermitian systems, Phys. Rev. A **99**, 032109 (2019).

[59] J. Dalibard, F. Gerbier, G. Juzeliūnas, and P. Öhberg, Colloquium: Artificial gauge potentials for neutral atoms, Rev. Mod. Phys. **83**, 1523 (2011).

[60] R. O. Umucalılar and I. Carusotto, Artificial gauge field for photons in coupled cavity arrays, Phys. Rev. A **84**, 043804 (2011).

[61] S. Mittal, J. Fan, S. Faez, A. Migdall, J. M. Taylor, and M. Hafezi, Topologically Robust Transport of Photons in a Synthetic Gauge Field, Phys. Rev. Lett. **113**, 087403 (2014).

[62] K. Fang, Z. Yu, and S. Fan, Realizing effective magnetic field for photons by controlling the phase of dynamic modulation, Nat. Photonics **6**, 782 (2012).

[63] M. Schmidt, S. Kessler, V. Peano, O. Painter, and F. Marquardt, Optomechanical creation of magnetic fields for photons on a lattice, Optica **2**, 635 (2015).

[64] P. Roushan *et al.*, Chiral ground-state currents of interacting photons in a synthetic magnetic field, Nat. Phys. **13**, 146 (2017).

[65] D. Leykam, S. Mittal, M. Hafezi, and Y. D. Chong, Reconfigurable Topological Phases in Next-Nearest-Neighbour Coupled Resonator Lattices, Phys. Rev. Lett. **121**, 023901 (2018).
[66] S. Mittal, W. DeGottardi, and M. Hafezi, Topological photonic systems, Opt. Photonics News **29**, 36 (2018).
[67] J. Garrison and E. Wright, Complex geometrical phases for dissipative systems, Phys. Lett. A **128**, 177 (1988).
[68] J. Zak, Berry's Phase for Energy Bands in Solids, Phys. Rev. Lett. **62**, 2747 (1989).
[69] D. C. Brody, Biorthogonal quantum mechanics, J. Phys. A **47**, 035305 (2014).
[70] R. El-Ganainy, K. G. Makris, M. Khajavikhan, Z. H. Musslimani, S. Rotter, and D. N. Christodoulides, Non-Hermitian physics and PT symmetry, Nat. Phys. **14**, 11 (2018).
[71] B. Zhu, R. Lü, and S. Chen, $\mathcal{PT}$ symmetry in the non-Hermitian Su-Schrieffer-Heeger model with complex boundary potentials, Phys. Rev. A **89**, 062102 (2014).
[72] M. Klett, H. Cartarius, D. Dast, J. Main, and G. Wunner, Relation between $\mathcal{PT}$-symmetry breaking and topologically nontrivial phases in the Su-Schrieffer-Heeger and Kitaev models, Phys. Rev. A **95**, 053626 (2017).
[73] B. Kramer and A. MacKinnon, Localization: Theory and experiment, Rep. Prog. Phys. **56**, 1469 (1993).
[74] F. Evers and A. D. Mirlin, Anderson transitions, Rev. Mod. Phys. **80**, 1355 (2008).
[75] M. Born and V. Fock, Beweis des adiabatensatzes, Z. Phys. **51**, 165 (1928).
[76] A. Messiah, *Quantum Mechanics* (North-Holland, Amsterdam, 1976).
[77] S. Longhi, Adiabatic passage of light in coupled optical waveguides, Phys. Rev. E **73**, 026607 (2006).
[78] R. Menchon-Enrich, A. Benseny, V. Ahufnger, A. D. Greentree, T. Busch, and J. Mompart, Spatial adiabatic passage: A review of recent progress, Rep. Prog. Phys. **79**, 074401 (2016).
[79] S. Longhi, Optical realization of multilevel adiabatic population transfer in curved waveguide arrays, Phys. Lett. A **359**, 166 (2006).
[80] A. A. Rangelov and N. V. Vitanov, Achromatic multiple beam splitting by adiabatic passage in optical waveguides, Phys. Rev. A **85**, 055803 (2012).
[81] C. Ciret, V. Coda, A. A. Rangelov, D. N. Neshev, and G. Montemezzani, Broadband adiabatic light transfer in optically induced waveguide arrays, Phys. Rev. A **87**, 013806 (2013).
[82] R. Uzdin, A. Mailybaev, and N. Moiseyev, On the observability and asymmetry of adiabatic state flips generated by exceptional points, J. Phys. A **44**, 435302 (2011).
[83] J. Doppler, A. A. Mailybaev, J. Böhm, U. Kuhl, A. Girschik, F. Libisch, T. J. Milburn, P. Rabl, N. Moiseyev, and S. Rotter, Dynamically encircling an exceptional point for asymmetric mode switching, Nature (London) **537**, 76 (2016).
[84] A. U. Hassan, G. L. Galmiche, G. Harari, P. LiKamWa, M. Khajavikhan, M. Segev, and D. N. Christodoulides, Chiral state conversion without encircling an exceptional point, Phys. Rev. A **96**, 052129 (2017).
[85] B. Midya, H. Zhao, and L. Feng, Non-Hermitian photonics promises exceptional topology of light, Nat. Commun. **9**, 2674 (2018).
[86] J. Gong, and Q. Wang, Piecewise adiabatic following in non-Hermitian cycling, Phys. Rev. A **97**, 052126 (2018).
[87] Y. E. Kraus, Y. Lahini, Z. Ringel, M. Verbin, and O. Zilberberg, Topological States and Adiabatic Pumping in Quasicrystals, Phys. Rev. Lett. **109**, 106402 (2012).
[88] M. Atala, M. Aidelsburger, J. T. Barreiro, D. Abanin, T. Kitagawa, E. Demler, and I. Bloch, Direct measurement of the Zak phase in topological Bloch bands, Nat. Phys. **9**, 795 (2013).
[89] S. Nakajima, T. Tomita, S. Taie, T. Ichinose, H. Ozawa, L. Wang, M. Troyer, and Y. Takahashi, Topological Thouless pumping of ultracold fermions, Nat. Phys. **12**, 296 (2016).
[90] C. H. Lee, S. Imhof, C. Berger, F. Bayer, J. Brehm, L. W. Molenkamp, T. Kiessling, and R. Thomale, Topolectrical circuits, Commun. Phys. **1**, 39 (2018).
[91] S. Longhi, Non-Hermitian tight-binding network engineering, Phys. Rev. A **93**, 022102 (2016).